

# Changes in Earth's Reflectance over the Past Two Decades

E. Pallé,<sup>1\*</sup> P. R. Goode,<sup>1,2</sup> P. Montañés-Rodríguez,<sup>1</sup> S. E. Koonin<sup>2</sup>

We correlate an overlapping period of earthshine measurements of Earth's reflectance (from 1999 through mid-2001) with satellite observations of global cloud properties to construct from the latter a proxy measure of Earth's global shortwave reflectance. This proxy shows a steady decrease in Earth's reflectance from 1984 to 2000, with a strong climatologically significant drop after 1995. From 2001 to 2003, only earthshine data are available, and they indicate a complete reversal of the decline. Understanding how the causes of these decadal changes are apportioned between natural variability, direct forcing, and feedbacks is fundamental to confidently assessing and predicting climate change.

The increase in global mean surface temperature over the past 50 years is believed to result in large part from the anthropogenic intensification of the atmospheric greenhouse effect. Although greenhouse gases modulate Earth's long-wave [infrared (IR)] emission, Earth's climate also depends on the net absorbed shortwave (SW) solar energy as quantified by the solar constant and Earth's albedo (the fraction of sunlight reflected back into space). The 0.1% variation of the solar constant over the 11-year solar cycle is widely regarded as insufficient to account for the present warming (1). However, it is not unreasonable to expect that changes in Earth's climate would induce changes in Earth's albedo and vice versa. Earth's surface, atmospheric aerosols, and clouds all reflect some of the incoming solar radiation, preventing that energy from warming the planet. Any changes in these components would likely change the albedo but would also induce climate feedbacks that complicate efforts to precisely assess causes and effects (2). The past two decades have seen some efforts to measure and monitor Earth's albedo from space with successful missions such as the Earth Radiation Budget Experiment (ERBE) or the Clouds and the Earth's Radiant Energy System (CERES) mission (3). However, a continuous long-term record of Earth's albedo is difficult to obtain because of the complex intercalibration of the various satellite data and the long temporal gaps in the series.

Over the past 5 years, we have been monitoring Earth's SW reflectance from Big Bear Solar Observatory (BBSO) by observing earthshine (ES): the ghostly glow of the dark portion of the lunar disk.

Earthshine is light reflected by Earth's sunlit hemisphere toward the Moon, and then retroreflected from the lunar surface. From the brightness of the earthlit Moon relative to that of the sunlit Moon (approximately  $10^{-4}$ ), one can precisely determine the large-scale reflectance of Earth (4–7). The modern earthshine approach yields an average albedo that is consistent with those determined by satellite missions (4–7).

From each night of ES observations, we deduced a value of Earth's apparent albedo,  $p^*$ , with roughly 1% precision. This quantity depends on the Sun-Earth-Moon geometry (the lunar phase angle), the geographical regions contributing to ES (that is, those por-

tions of Earth that are simultaneously visible from the Sun and Moon), and the weather in those regions on that day (clouds, snow/ice, etc.). The apparent albedo can be understood as Earth's reflectance in one direction, whereas its average over all directions is the Bond albedo (roughly 0.3) (6). Although we cannot determine a precise value of the Bond albedo on daily time scales (6), we can study its longer-term variation by averaging the daily anomalies,  $\Delta p^*$ , with respect to their mean (also roughly 0.3) at each lunar phase (7).

Our analysis began by determining which regions of Earth contributed to ES during each night of 1999–2001 BBSO observation (observation was typically 2 to 4 hours in duration). We then determined average cloud and surface properties for that region and time from the International Satellite Cloud Climatology Project (ISCCP) D1 daily data set (Fig. 1). The spatial averages we calculated were weighted by the surface area of each ISCCP cell, doubly projected on the Sun and Moon directions (7). For a complete description of the ISCCP products, see (8). The present ISCCP data release covers the period from July 1983 to September 2001, and it is expected to be updated in the near future (9).

To relate our  $\Delta p^*$  measurements to ISCCP data, we performed a linear multiple regression with  $\Delta p^*$  as a variable dependent on several ISCCP cloud parameters. Because reflection anisotropies will cause the relation between cloud properties and  $\Delta p^*$  to change with lunar

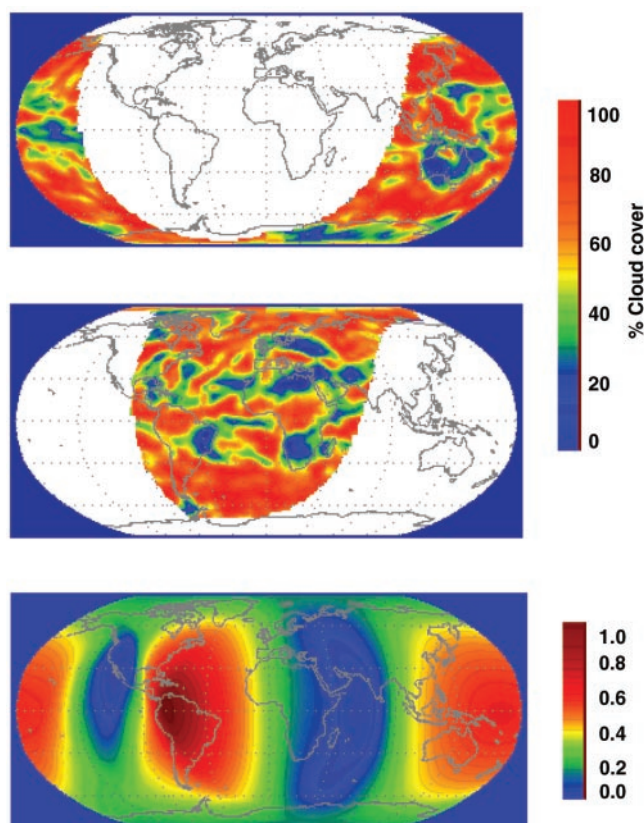


**Fig. 1.** Mean cloud cover map for 15 October 1999 (top) and 4 September 1999 (middle) over the area contributing to ES during about 4 hours of observation from BBSO each night. The mean lunar phases were  $-115.8^\circ$  (waxing) and  $+109.7^\circ$  (waning), respectively. Such coverages are typical for a single night's observations. (Bottom) The weighted contribution of each part of Earth to the ES observations during the 1999–2001 period. The arbitrary normalized scale reflects the number of times that each area of Earth has contributed to ES, weighted by the Earth-Moon cosine at each observation. The darker blue areas are those we cannot see in ES from California.

<sup>1</sup>Big Bear Solar Observatory, New Jersey Institute of Technology, 40386 North Shore Lane, Big Bear City, CA 92314, USA. <sup>2</sup>W. K. Kellogg Radiation Laboratory, California Institute of Technology, Pasadena, CA 91125, USA.

\*To whom correspondence should be addressed. E-mail: epb@bbso.njit.edu

phase, we performed a separate regression for each of 14 contiguous lunar phase bins 10° wide, covering from 65° to 135° for both positive and negative phase angles. Initially, we selected from the ISCCP parameters those that we thought would have a greater impact on Earth's reflectance: cloud height, surface reflectance (SR), cloud-top optical thickness (OT), mean cloud amount (CA), cloud-top temperature and pressure, mean IR cloud amount, and the several visible and IR cloud type subdivisions. Although none of the selected ISCCP cloud variables alone correlated at any statistically significant level with  $\Delta p^*$ , SR, OT, and CA (in order of decreasing correlation) had the strongest correlation in all bins. Thus, we selected these three independent variables to perform the multiple regression. The regression is more than 99% significant for all but three of the lunar phase bins (in which it is only 80 to 90% significant). Our data cover about one-third of each lunar month; for phases outside this range, sparse data make the regression unreliable (6).

We express the apparent albedo anomaly as

$$\Delta p^* = c_0 + (c_1 \times CA) + (c_2 \times OT) + (c_3 \times SR) \quad (1)$$

where CA, OT, and SR are averaged over the night's ES-contributing area. The regression coefficients,  $c_i$ , are independently calculated for each lunar phase bin. Nevertheless, they are similar for positive and negative lunar phases of the same magnitude and vary smoothly with lunar phase; these results reinforce our confidence in the analysis.

From 1999 through mid-2001, we have both ISCCP and ES data on 310 observing nights for which we can compare reconstructed and observed  $\Delta p^*$ 's (Fig. 2). Although the empirical and reconstructed values differ on some nights, the overall agreement is quite good ( $r = 0.6$ ,  $P \ll 0.001$ ).

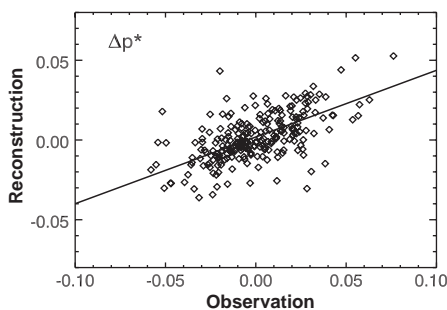


**Fig. 2.** Scatter plot of the measured versus reconstructed  $p^*$  anomalies on the 310 nights during 1999–2001 for which both ES observations and ISCCP data are available. The diagonal line represents the best linear fit to the data. In general, the observations vary more widely about the mean than do the reconstructed values. Variations in cloud properties over the averaged area with respect to the mean and the nonlinearity of cloud albedo with optical depth contribute to the scatter among these points.

Our regressions then allow us to construct an ISCCP-derived proxy for Earth's reflectance at times when ES data are not available. In particular, we can reconstruct the albedo on dates since 1999 until mid-2001 when local clouds or equipment problems prevented observations from BBSO. Further, we can confidently extrapolate back to the first ISCCP data (July 1983) by determining what the ES observing times would have been (based on the lunar phase and our observing capabilities) and thus what regions of Earth would have contributed to ES. The reconstructed annual mean  $p^*$  anomaly ( $\Delta p^*$ ) from 1984 to 2000 is plotted in Fig. 3.

Quite evident in Fig. 3 is the fairly steady decrease in reconstructed reflectance from the late 1980s to the late 1990s. Support for this trend and for the regression comes from BBSO ES observations during 73 nights of 1994 and 1995. Because these were performed with slightly different instrumentation than that used in later years, those data were not used in the regression. Nevertheless, the roughly 2% excess of Earth's apparent reflectance in the 1994–1995 period relative to 1999–2001 is in good agreement with the reconstruction from ISCCP data.

The albedos for the years after the eruption of Mt. Pinatubo (1991–1992) are among the largest; however, the increase is just comparable with interannual variability. The lack of a sharp rise is not unexpected, however, because Pinatubo's increased contribution of stratospheric aerosols is not accounted for by any of the ISCCP parameters used. Nor are there any apparent signatures of El Niño–Southern Oscillation events, perhaps because of near-cancellation of opposing effects over the wide longitudinal areas sampled by ES measurements.

The decrease in Earth's reflectance from 1984 to 2000 suggested by ISCCP data in Fig. 3 corresponds to a change in  $p^*$  of some  $-0.02$ , which translates into a decrease of the Bond albedo by 0.02 ( $\Delta p^*/p^* = \Delta A/A$ ) (7) and an additional SW absorption,  $R$ , of 6.8  $W/m^2$  ( $R = \Delta A \times C/4$ , where  $C = 1368$   $W/m^2$  is the solar constant). This is climato-

logically very significant. For example, the latest IPCC report (10) argues for a 2.4  $W/m^2$  increase in  $CO_2$  longwave forcing since 1850. Our observational ES data extend from 1999 to 2003 and indicate a clear reversal of the ISCCP-derived reflectance trend starting in 1999 up through 2003. The increasing trend in reflectance corresponds to approximately 5  $W/m^2$ , bringing the mean reflectance anomaly back to its 1980s values. Only the ES data are currently available to signal this reversal; it will be interesting to see how the proxy behaves when ISCCP data are available beyond mid-2001.

To ascertain that the variation of the proxy in Fig. 3 is due to changes in cloud properties, we have done mock reconstructions of  $\Delta p^*$ , both with fixed ISCCP maps and separately with random scrambles of the 18-year ISCCP daily data set. The average of several random reconstructions and the reconstruction with fixed ISCCP parameters are virtually indistinguishable and vary only because of the superposition of several smaller lunar orbital cycles that are imperfectly accounted for in the linear regression. However, the resulting corrections implied are two orders of magnitude smaller than the observed variability.

The ES sampling, and thus our reconstruction, is incomplete because we can only determine Earth's reflectance on certain days and at certain times. However, the proxy variation in Fig. 3 is not a result of this sampling. To demonstrate this, we artificially shifted the days (and times) of our ES observations, so that different ISCCP subsets were used within their proper, or adjacent, lunar months; the results in Fig. 3 did not change. Further, if the reconstructed series is divided between positive and negative lunar phases, the variation of the two subsets remains comparable to that in Fig. 3.

Some recent studies using an intercalibration of several satellite data sets have reported strong trends over the tropical regions in both (increasing) outgoing long-wave radiation (OLR) and (decreasing) reflected SW radiation (11, 12). Taken at face value, these results seem

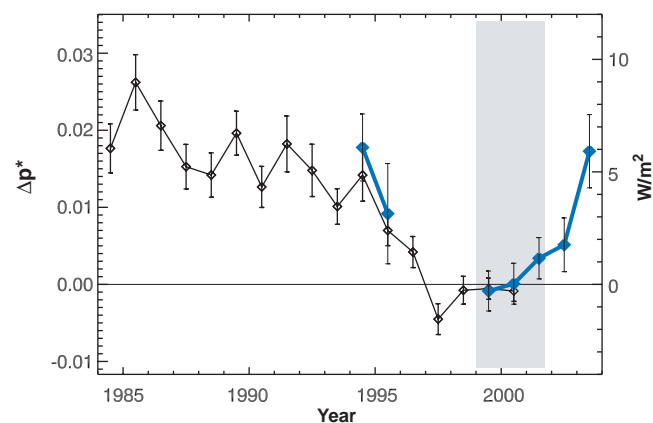


**Fig. 3.** Reconstructed annual reflectance anomalies,  $\Delta p^*$  (black), with respect to the mean anomaly for the regression calibration period 1999–2001 (vertical gray band). The large error bars result from the seasonal variability of Earth's albedo, which can be 15 to 20% (3, 6). Also plotted (blue) are the ES-observed annual anomalies for 1999–2003 and 1994–1995. The right-hand vertical scale shows the deficit in global SW forcing relative to 1999–2001.

to suggest an increased cooling rate of the global surface and troposphere, because their estimated  $\sim 5 \text{ W/m}^2$  increase in OLR radiation (implied cooling) over the period 1985–2000 is larger than the  $\sim 2 \text{ W/m}^2$  SW decrease (implied warming) over the same period (11, 13). Our results for SW radiation are broadly consistent with these studies on a quasi-global scale, although we are somewhat biased toward the tropical regions because of the geometry inherent in ES measurements (Fig. 1). However, the albedo decrease of the proxy is two to three times larger than the satellite estimates, making it comparable to their estimated decrease in OLR (11). The post-1999 recovery we find is a novel result.

The effect of clouds on Earth's albedo is probably larger in visible light than in the ultraviolet (UV) or near-IR. For UV radiation, strong Rayleigh scattering and ozone absorption reduce the impact of clouds on the albedo. In the near-IR region, absorption by cloud particles, water vapor, and carbon dioxide all limit the impact. Consequently, variations in broadband SW albedo may be somewhat smaller than those in the visible albedo shown in Fig. 3.

If the changes in cloud properties responsible for the reflectance changes shown by the proxy were a result of secularly increasing atmospheric greenhouse gases, then they would signal a strong positive SW cloud feedback, although a simultaneous negative feedback may be expected through reduced cloud trapping of IR radiation (14). However, the reflectance increase from 1999 to 2003 would be difficult to attribute to monotonically increasing atmospheric greenhouse gases. Natural variability is a much more plausible explanation, given the size and time scale of the proxy changes.

We have used a combination of ES and satellite observations to deduce interannual and decadal variations in Earth's large-scale reflectance. A decreasing reflectance since 1984 is derived from the ISCCP data, with a sharp drop during the 1990s. However, the ES data available for subsequent years, with as yet no corresponding ISCCP data, indicate that the trend has reversed since 1999, with the decline being largely erased by the end of 2003. These large variations in reflectance imply climatologically significant cloud-driven changes in Earth's radiation budget, which is consistent with the large tropospheric warming that has occurred over the most recent decades. Moreover, if the observed reversal in Earth's reflectance trend is sustained during the next few years, it might also play a very important role in future climate change. The ability of climate models to reproduce changes such as these (whether due to natural variability or anthropogenic forcing) is therefore an important test of our ability to assess and predict climate change.

#### References and Notes

1. J. Lean, *Annu. Rev. Astron. Astrophys.* **35**, 33 (1997).
2. R. D. Cess et al., *J. Geophys. Res.* **101**, 12791 (1996).
3. The ERBE instruments were flown on the ERBS,

- NOAA-9, and NOAA-10 satellites from late 1984 to 1990 (asd-www.larc.nasa.gov). ScaRab/Meteor and ScaRab/Ressur also measured Earth's albedo during 1994–1995 and 1998–1999, respectively (www.lmd.polytechnique.fr/~Scarab/). In 1998, CERES began taking albedo measurements (asd-www.larc.nasa.gov/ceres/), and the Geostationary Earth Radiation Budget Experiment (GERB), the first broadband radiometer on a geostationary satellite, has been in operation since December 2002 (www.sp.ph.ic.ac.uk/gerb/). The future satellite missions EARTHSHINE (www.sstd.rl.ac.uk) and TRIANA (on hold) (triana.gsfc.nasa.gov) may also contribute by observing the full Earth disk reflectance from the privileged deep-space position of the L1 Lagrange point.
4. P. R. Goode et al., *Geophys. Res. Lett.* **28**, 1671 (2001).
5. When referring to SW reflectance as observed by ES, we mean the visible region from 400 to 700 nm covered by our detector.
6. J. Qiu et al., *J. Geophys. Res.* **108**, 4709, 10.1029/2003JD003610 (2003).
7. E. Pallé et al., *J. Geophys. Res.* **108**, 4710, 10.1029/2003JD003611 (2003).
8. W. B. Rossow, A. W. Walker, D. E. Beusichel, M. D. Roiter, *International Satellite Cloud Climatology Project (ISCCP): Documentation of New Cloud Data-*

sets (WMO/TD-No. 737, World Meteorological Organization, Geneva, Switzerland, 1996).

9. The latest ISCCP data, documentation, and related information can be downloaded from the ISCCP Web site at <http://isccp.giss.nasa.gov>.
10. Intergovernmental Panel on Climate Change (IPCC), *Climate Change 2001: The Scientific Basis. Contribution of Working Group I to the Third Assessment Report of the Intergovernmental Panel on Climate Change (IPCC)*, J. T. Houghton et al., Eds. (Cambridge Univ. Press, Cambridge, 2001).
11. B. A. Wielicki et al., *Science* **295**, 841 (2002).
12. P. Wang, P. Minnis, B. A. Wielicki, T. Wong, L. B. Vann, *Geophys. Res. Lett.* **29**, 10.1029/2001GL014264 (2002).
13. J. Chen, B. E. Carlson, A. D. Del Genio, *Science* **295**, 838 (2002).
14. R. D. Cess, P. M. Udelhofen, *Geophys. Res. Lett.* **30**, 1019 (2003).
15. This research was supported in part by a grant from NASA (NAG5-11007). The cloud ISCCP D1 data sets were obtained from the NASA Langley Research Center Atmospheric Sciences Data Center. We are grateful to Y. Yung, B. Soden, T. Schneider, and five anonymous referees for their comments on drafts of this paper.

26 November 2003; accepted 21 April 2004

## Elastic Behavior of Cross-Linked and Bundled Actin Networks

M. L. Gardel,<sup>1</sup> J. H. Shin,<sup>3,4</sup> F. C. MacKintosh,<sup>5</sup> L. Mahadevan,<sup>2</sup> P. Matsudaira,<sup>4</sup> D. A. Weitz<sup>1,2\*</sup>

Networks of cross-linked and bundled actin filaments are ubiquitous in the cellular cytoskeleton, but their elasticity remains poorly understood. We show that these networks exhibit exceptional elastic behavior that reflects the mechanical properties of individual filaments. There are two distinct regimes of elasticity, one reflecting bending of single filaments and a second reflecting stretching of entropic fluctuations of filament length. The mechanical stiffness can vary by several decades with small changes in cross-link concentration, and can increase markedly upon application of external stress. We parameterize the full range of behavior in a state diagram and elucidate its origin with a robust model.

Actin is a ubiquitous protein that plays a critical role in virtually all eukaryotic cells. It is a major constituent of the cytoskeletal network that is an essential mechanical component in a variety of cellular processes, including motility, mechanoprotection, and division (1, 2). The mechanical properties, or elasticity, of these cytoskeletal networks are intimately involved in determining how forces are generated and transmitted in living cells. In vitro, actin can polymerize to form long rigid filaments (F-actin), with a diameter  $D \approx 7 \text{ nm}$  and contour lengths up to  $L \approx 20 \text{ }\mu\text{m}$  (3). Despite their rigidity, thermal effects nevertheless modify the

dynamic configuration of actin filaments, leading to bending fluctuations. The length scale where these fluctuations completely change the direction of the filament is the persistence length,  $\ell_p = \kappa_o/k_B T \approx 17 \text{ }\mu\text{m}$ , determined when the bending energy equals the thermal energy; here,  $\kappa_o$  is the bending modulus of the actin filament. Entangled solutions of F-actin are a well-studied model for semiflexible polymers; they exhibit exceptionally large elasticity at small volume fractions as compared with more traditional flexible polymers at similar concentrations (4–6). However, in vivo, the cytoskeletal network is regulated and controlled not only by the concentration of F-actin, but also by accessory proteins that bind to F-actin. Indeed, nature provides a host of actin-binding proteins (ABPs) with a wide range of functions: They can align actin filaments into bundles and they can cross-link filaments or bundles into networks (2, 7). However, unlike flexible polymers, where changes in cross-link density do not markedly affect the elasticity (8), small changes in the concentration of cross-linker ABPs dramatically alter the elasticity of F-actin

<sup>1</sup>Department of Physics, <sup>2</sup>Division of Engineering and Applied Sciences, Harvard University, Cambridge, MA 02138, USA. <sup>3</sup>Department of Mechanical Engineering, Massachusetts Institute of Technology (MIT), Cambridge, MA 02139, USA. <sup>4</sup>Department of Biology and Division of Biological Engineering, Whitehead Institute for Biomedical Research, MIT, Cambridge, MA 02142, USA. <sup>5</sup>Division of Physics and Astronomy, Vrije Universiteit, Amsterdam, Netherlands.

\*To whom correspondence should be addressed. E-mail: weitz@deas.harvard.edu